

Contents lists available at ScienceDirect

## Comput. Methods Appl. Mech. Engrg.

journal homepage: www.elsevier.com/locate/cma



# Hybridized augmented Lagrangian methods for contact problems

Erik Burman<sup>a</sup>, Peter Hansbo<sup>b</sup>, Mats G. Larson<sup>c</sup>

- <sup>a</sup> Mathematics, University College London, UK
- <sup>b</sup> Mechanical Engineering, Jönköping University, Sweden
- <sup>c</sup> Mathematics and Mathematical Statistics, Umeå University, Sweden

### ARTICLE INFO

### Keywords: Elastic contact Augmented Lagrangian Hybridization

### ABSTRACT

This paper addresses the problem of friction-free contact between two elastic bodies. We develop an augmented Lagrangian method that provides computational convenience by reformulating the contact problem as a nonlinear variational equality. To achieve this, we propose a Nitschebased method incorporating a hybrid displacement variable defined on an interstitial layer. This approach enables complete decoupling of the contact domains, with interaction occurring exclusively through the interstitial layer. The layer is independently approximated, eliminating the need to handle intersections between unrelated meshes. Additionally, the method supports introducing an independent model on the interface, which we leverage to represent a membrane covering one of the bodies as well as a plate resting on one of the bodies. We present the formulation of the method, establish stability and error estimates, and demonstrate its practical utility through illustrative numerical examples.

### 1. Introduction

Traditionally, two-body contact algorithms in finite element analysis rely on a node-to-segment approach, where the nodes of one mesh are constrained from crossing the discrete boundary of the other. In a one-pass algorithm, only the nodes on one of the surfaces are considered, which can result in local penetration if the mesh densities differ significantly. A two-pass algorithm, on the other hand, considers nodes on both surfaces, but this can lead to ill-posed problems, cf. El-Abbasi and Bathe [1]. This arises when nodes on the two surfaces are very close, as they may impose nearly identical contact conditions. To address this issue, additional checks are necessary, as discussed by Puso and Laursen [2].

The contact constraints can be enforced using discrete Lagrange multipliers (contact pressures) associated with the nodes or a nodal penalty method that penalizes the no-penetration constraint. Another classical approach is the distributed Lagrange multiplier method [1,3], where the multiplier's discretization is typically related to the surface mesh of one of the bodies to ensure stability. Consequently, these approaches require careful handling of intersections between unrelated meshes. This challenge also applies to distributed penalty methods and Nitsche's method.

To overcome these limitations and enable a more flexible approximation of the interface variables, we extend the hybrid Nitsche's method [4,5], which incorporates an independent displacement field at the interface, to the case of friction-free elastic contact. The hybrid field can serve as an auxiliary variable without direct physical interpretation, facilitating the transfer of information between the contacting bodies. For instance, the hybrid field may be defined on a structured mesh for computational convenience. Another advantages of a hybrid Nitsche method, as compared to the standard Nitsche method, is that it makes it convenient to eliminate internal degrees of freedom in a parallel fashion so that the linear system can be solved by iterative substructuring methods, as

E-mail addresses: e.burman@ucl.ac.uk (E. Burman), peter.hansbo@ju.se (P. Hansbo), mats.larson@umu.se (M.G. Larson).

https://doi.org/10.1016/j.cma.2025.118175

Received 28 January 2025; Received in revised form 28 May 2025; Accepted 19 June 2025

Available online 4 July 2025

0045-7825/© 2025 The Authors. Published by Elsevier B.V. This is an open access article under the CC BY license (http://creativecommons.org/licenses/by/4.0/).

<sup>\*</sup> Corresponding author.

discussed by Gustavsson et al. [6]. In the context of contact problems, however, the most interesting feature of the method lies in the possibility of defining a model for the interface variable, such as a membrane covering one of the bodies or a shell located between the two bodies. If this is to be done using Lagrange multipliers, the cost increases as two sets of multipliers must be used, coupling the interface model from both sides of the contact zone. Model coupling is thus the focus of this paper.

We formulate the hybrid approach within an augmented Lagrangian framework, leveraging Rockafellar's reformulation [7–9] of the well-known Kuhn–Tucker contact conditions. For Nitsche's method this reformulation was first proposed and analyzed by Chouly and Hild [10], in the context of friction-free contact. This framework enables the definition of the Nitsche stabilization mechanism for variational inequality problems, transforming the inequality constraints associated with contact into nonlinear *equalities* (see also [11]). These equalities facilitate the application of iterative solution schemes in the spirit of Alart and Curnier [12]. We establish theoretical results, including stability and approximation properties, to support the method's robustness. Finally, we provide several numerical examples to demonstrate our method's practical application and performance.

### 1.1. Relation to previous work and outline

For a general overview of computational methods for contact we refer to [13]. Our method shares similarities with that of Chouly and Hild [10] and the developments thereof [14–16], but with a significant distinction: it allows for an independent approximation of the displacement field in the contact zone, decoupled from the approximation used in the elastic bodies. Nitsche's method and related stabilized Lagrange multiplier methods have been analyzed for contact problems also in [17], where estimates were proved requiring no additional solution regularity.

The method we propose is also related to domain decomposition methods for contact problems. The pioneering works in for this approach were using Schwarz methods [18] or FETI methods [19]. Our work is more closely related to mortar methods combined with the Augmented Lagrangian method [20]. We refer to [11] for a discussion of the relation between the Augmented Lagrangian method and Nitsche's method in the context of variational inequalities. For other work on mortar methods for contact problems we refer to [2,21–25]. Recent work has also explored mortar methods with NURBS or IGA, we refer to [26–28]. Another popular domain decomposition approach is the LaTin framework. For works relevant in our context we refer to [29,30] and more recently [31]. In the latter reference it is underlined that different coupling conditions can be integrated easily by changing the coupling form. Similarly to such methods the ideas we propose integrate seamlessly in the cutFEM framework combining the ideas of [32,33]. To the best of our knowledge however none of these references introduce mixed dimensional pde problems to handle interstitial layers with mechanical properties.

The structure of the paper is as follows: Section 2 introduces the contact model, derives the hybridized finite element method, and formulates the associated optimality equations. Section 3 presents a stability estimate, a best approximation result, and a discussion of the method's convergence order. Section 4 provides several numerical examples to illustrate the practical application and performance of the method. Section 5 concludes the paper with a summary of key findings and insights.

### 2. A contact model problem

### 2.1. Hybridized problem formulation

We shall study several different contact problems between two elastic bodies occupying the domains  $\Omega_i \subset \mathbb{R}^d$ , i=1,2, with d=2 or 3. Let  $\Omega_0$  denote a hybrid object located between  $\Omega_1$  and  $\Omega_2$ , see Fig. 1. For d=3, the hybrid object is a surface, and for d=2, it is a curve. The bodies  $\Omega_1$  and  $\Omega_2$  do not come into direct contact; all interactions are mediated through  $\Omega_0$ . Thus, all information exchanged between  $\Omega_1$  and  $\Omega_2$  passes through the hybrid space. We will consider two scenarios:

- Case 1. The hybrid space is an auxiliary tool to facilitate numerical computations. For example, it may consist of a structured mesh that efficiently transfers data between two unstructured meshes. In this scenario, the hybrid space must be stabilized, potentially by ensuring it conforms to the boundary of one of the bodies.
- Case 2. The hybrid space represents physical interactions between  $\Omega_1$  and  $\Omega_2$ , such as a membrane or a plate residing between them, as described in [34].

In both cases, the hybrid object  $\Omega_0$  is treated as the master object, while the elastic bodies  $\Omega_i$ , i = 1, 2, implement contact or equality constraints. The hybrid object is only influenced by the normal stresses exerted by the two elastic bodies.

We will demonstrate that both cases can be conveniently addressed and analyzed within a unified abstract framework. To achieve this, we will not initially specify the exact properties of the forms associated with the hybrid object. Instead, we will develop the analysis based on general abstract assumptions and define the specific hybrid forms for the applications presented below. This approach emphasizes the flexibility and generality of the framework.

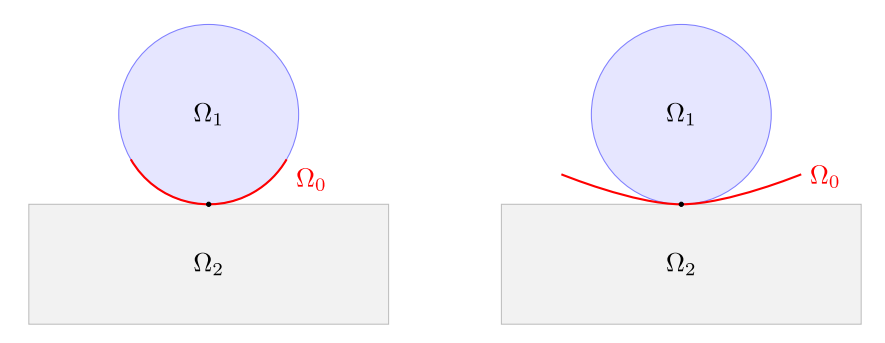


Fig. 1. Left: Case 1, hybrid space an auxiliary space weakly constrained to follow the boundary of one of the active bodies. Right: Case 2, hybrid space representing physics.

Governing equations for the elastic bodies. Following the problem definition of Fabre, Pousin, and Renard [35], the boundary  $\partial\Omega_i$  of  $\Omega_i$ , for i=1,2, is divided into three nonoverlapping parts:  $\partial\Omega_{i,C}$  (the potential zone of contact),  $\partial\Omega_{i,N}$  (the Neumann part), and  $\partial\Omega_{i,D}$  (the Dirichlet part) which we, in the analysis, assume have non-zero measure to guarantee that Korn's inequality holds. We let  $n_i$  be the exterior unit normal to  $\partial\Omega_i$ .

Let  $u_i: \Omega_i \to \mathbb{R}^d$  denote the displacement field on  $\Omega_i$ . We assume that the two elastic bodies  $\Omega_i$ , i = 1, 2, are subjected to volume forces  $f_i$  and, for simplicity, zero displacements on  $\partial \Omega_{i,D}$  and zero tractions on  $\partial \Omega_{i,N}$ ,

$$-\nabla \cdot \boldsymbol{\sigma}(\boldsymbol{u}_i) = \boldsymbol{f}_i \quad \text{in } \Omega_i$$

$$\mathbf{u}_i = \mathbf{0}$$
 on  $\partial \Omega_{i,D}$  (2)

$$\sigma_n(\mathbf{u}_i) = \mathbf{0}$$
 on  $\partial \Omega_{i,N}$  (3)

We further assume that Hooke's constitutive law holds

$$\sigma(u_i) = \lambda_i \operatorname{tr} \varepsilon(u_i) \mathbf{I} + 2\mu_i \varepsilon(u_i), \qquad \varepsilon(u_i) = \frac{1}{2} (u_i \otimes \nabla + \nabla \otimes u_i)$$
(4)

with Lamé parameters  $\mu_i$  and  $\lambda_i$ . We must add the equality or contact constraints on  $\partial \Omega_{i,C}$  to complete the equations.

The equality and inequality constraints. To define our contact constraints, we start by defining the distance between  $\Omega_i$  and  $\Omega_0$ ,

$$\rho_{i,0}(z) = (n_{i,0}(z), z - p_0(z))_{\mathbb{R}^d} \tag{5}$$

where  $z \in \partial \Omega_{i,C}$ ,  $p_0(z)$  is the closest point mapping associated with  $\Omega_0$ , and  $n_{i,0}(z) = n_{i,0}(p_0(z))$  is the pullback of the normal to  $\Omega_0$  pointing into  $\Omega_i$ , cf. Fig. 2. Taking the deformation fields  $v_i$  on  $\Omega_i$  and  $v_0$  on  $\Omega_0$  into account by replacing  $z - p_0(z)$  by  $(z + v_i(z)) - (p_0(z) - v_0(p_0(z)))$ , gives

$$\widetilde{\rho}_{i,0}(z, v_0, v_i) = (n_{i,0}(z), z + v_i(z))_{\mathbb{R}^d} - (n_{i,0}(z), p_0(z) + v_0(p_0(z))_{\mathbb{R}^d}$$
(6)

$$= (\mathbf{n}_{i,0}(z), z - \mathbf{p}_0(z))_{\mathbb{R}^d} + (\mathbf{n}_{i,0}(z), \mathbf{v}_i(z) - \mathbf{v}_0(\mathbf{p}_0(z))_{\mathbb{R}^d}$$
(7)

$$= \rho_{i,0}(z) + (\mathbf{n}_{i,0}(z), \nu_i(z) - \nu_0(p_0(z))_{\mathbb{R}^d}$$
(8)

$$= \rho_{i,0}(z) - [v_n]_i \tag{9}$$

Thus, we may extend the definition (5) to the deformed case by

$$\widetilde{\rho}_{i,0}(z, \boldsymbol{v}_0, \boldsymbol{v}_i) = \rho_{i,0}(z) - [\boldsymbol{v}_n(z)]_i \quad \text{on } \partial\Omega_{i,C}$$

$$\tag{10}$$

where

$$[v_n(z)]_i = (n_{i,0}(z), v_i(z))_{\mathbb{R}^d} - (v_0(p_0(z))_{\mathbb{R}^d})$$
(11)

is the jump in the normal displacements. In the following, we make the dependence on z implicit and use the more compact notation  $\widetilde{\rho}_{i,0}(v_0,v_i)$  etc.

**Remark 2.1.** Note that the exterior unit normal to the elastic body satisfies  $n_i = -n_0$  in the contact zone and  $n_i \approx -n_0$  close to the contact if the boundary is smooth and thus

$$[v_n] \approx v_{i,n} + v_{0,n} = (n_i, v_i)_{\mathbb{R}^d} + (n_0, v_0)_{\mathbb{R}^d}$$
(12)

which is the standard definition of the jump in the normal displacement.

We then have the following constraints,

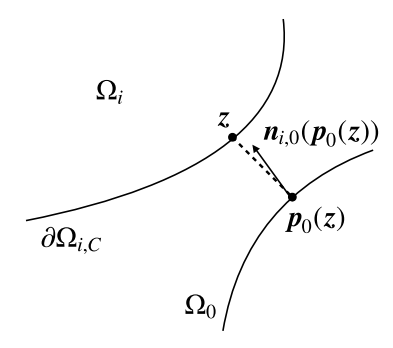


Fig. 2. Closest point  $p_0$  and normal  $n_{i,0}$ .

### · Hybridized equality constraint:

$$\widetilde{\rho}_{i,0}(u_i,u_0) = 0$$
 on  $\partial \Omega_{i,C}$  (13)

· Hybridized contact constraints:

$$-\tilde{\rho}_{i,0}(\mathbf{u}_i, \mathbf{u}_0) \le 0 \qquad \text{on } \partial\Omega_{i,C}$$

$$\tag{14}$$

$$\sigma_n(u_i) \le 0$$
 on  $\partial \Omega_{i,C}$  (15)

$$\sigma_n(\mathbf{u}_i)\widetilde{\rho}_i(\mathbf{u}_i,\mathbf{u}_0) = 0$$
 on  $\partial\Omega_{i,C}$  (16)

where  $\sigma_n(\mathbf{v})$  is the (scalar) normal surface stress

$$\sigma_n(v_i) = n_i \cdot \sigma(v_i) \cdot n_i \tag{17}$$

### 2.2. A hybrid Nitsche finite element method

Function and finite element spaces. We first define the natural function spaces for our continuous problem. Let  $V_i = H^1(\Omega_i)$  for i = 1, 2, and  $V_0 = H^{s_0}(\Omega_0)$  where  $s_0$  depends on the physical properties of the hybrid space. For convenience, we define the product space

$$W = V_0 \oplus V_1 \oplus V_2 \tag{18}$$

of  $\mathbb{R}^d$  valued displacement fields.

Next, we define the corresponding finite element spaces. To that end let  $\mathcal{T}_{h,i}$  be a quasi-uniform partition of  $\Omega_i$ , into shape regular elements T, with mesh-parameter  $h_i \in (0,h_0]$ . Let  $V_{h,i} \subset V_i$  be a conforming finite element space on  $\mathcal{T}_{h,i}$  consisting of piecewise polynomials of order  $p_i$ . Let  $\pi_{h,i}: H^1(\Omega_i) \to V_{h,i}$  be an interpolation operator such that

$$||v - \pi_{h,i}v||_{H^m(T)} \lesssim h_i^{k-m} ||v||_{H^k(N(T))}, \qquad 0 \le m \le k \le p_i + 1$$
 (19)

We finally define the product of the finite element spaces

$$W_h = V_{h,0} \oplus V_{h,1} \oplus V_{h,2}$$
 (20)

where  $V_{h,i}$  are the d-dimensional versions of the corresponding scalar spaces.

Augmented Lagrangian formulation. We consider the nonlinear augmented Lagrangian formulation of Rockafellar [7–9], introduced in contact analysis by Alart and Curnier [12]. The basic idea is to write the Kuhn–Tucker conditions (14)–(16) in the equivalent form

$$\sigma_{n}(u_{i}) = [\sigma_{n}(u_{i}) + \gamma_{i}\widetilde{\rho}_{i,0}(u_{0}, u_{i})]_{-} = [\sigma_{n}(u_{i}) - \gamma([u_{n}]_{i} - \rho_{i,0})]_{-}$$
(21)

where  $[x]_{-} = \min(x, 0)$  and  $\gamma > 0$  is a parameter, see Appendix and [10]. Dimensional analysis indicates that

$$\gamma_i = \gamma_0 h_i^{-1} \tag{22}$$

for a parameter  $\gamma_0$  not dependent on  $h_i$ , and we will see in the forthcoming analysis that this is indeed the proper choice. To handle equality and inequality constraints in the same formulation, we define

$$S_{i}(\mathbf{v}) = \begin{cases} \sigma_{n}(\mathbf{v}_{i}) - \gamma_{0} h_{i}^{-1}([v_{n}]_{i} - \rho_{i,0}) & \text{Equality} \\ [\sigma_{n}(\mathbf{v}_{i}) - \gamma_{0} h_{i}^{-1}([v_{n}]_{i} - \rho_{i,0})]_{-} & \text{Inequality} \end{cases}$$
(23)

Note that  $S_i(\mathbf{v})$  is a function of  $\mathbf{v}_0$  and  $\mathbf{v}_i$ , so that  $S_i(\mathbf{v}) = S_i(\mathbf{v}_i, \mathbf{v}_0)$ .

### Remark 2.2. The quantity

$$\Sigma_{n,i}(v_0, v_i) = \sigma_n(v_i) - \gamma_0 h_i^{-1}([v_n]_i - \rho_{i,0}) \tag{24}$$

is the so-called Nitsche normal stress, which is the natural approximation of the normal stress provided by the method and thus

$$S_{i}(\mathbf{v}) = \begin{cases} \Sigma_{n,i}(\mathbf{v}_{0}, \mathbf{v}_{i}) & \text{Equality} \\ [\Sigma_{n,i}(\mathbf{v}_{0}, \mathbf{v}_{i})]_{-} & \text{Inequality} \end{cases}$$
 (25)

We note that the inequality constraint only allows negative normal stress.

We can now formulate a discrete minimum problem

$$\boxed{\boldsymbol{u}_h = \operatorname{argmin}_{\boldsymbol{v}_h \in W_h} \mathcal{L}_A(\boldsymbol{v}_h)}$$
(26)

where, with

$$I_a = \begin{cases} \{1,2\} & \text{Case 1} \\ \{0,1,2\} & \text{Case 2} \end{cases}$$
 (27)

denoting the index set indicating the number of active forms in Case 1 (auxiliary hybrid space) and Case 2 (physical modeling hybrid space), the augmented Lagrangian takes the form

$$\mathcal{L}_{A}(\mathbf{v}) = \sum_{i \in I_{a}} \frac{1}{2} a_{i}(\mathbf{v}, \mathbf{v}) - l_{i}(\mathbf{v}) + \sum_{i=1}^{2} \frac{1}{2} \gamma_{0}^{-1} \|S_{i}(\mathbf{v})\|_{H_{h}^{-1/2}(\partial\Omega_{i,C})}^{2} - \frac{1}{2} \gamma_{0}^{-1} \|\sigma_{n}(\mathbf{v}_{i})\|_{H_{h}^{-1/2}(\partial\Omega_{i,C})}^{2}$$
(28)

Here, for i = 1, 2, the forms are defined by

$$a_i(\mathbf{v}, \mathbf{w}) = (\sigma_i(\mathbf{v}_i), \epsilon(\mathbf{w}_i))_{\Omega_i} \tag{29}$$

$$l_i(\mathbf{v}) = (f_i, v_i)_{\Omega_i} \tag{30}$$

and the forms  $a_0$  and  $l_0$  are related to the hybrid space and may model some physics (Case 2) or could be zero (Case 1). In the latter case,  $\Omega_0$  is connected weakly to  $\Omega_{i,C}$  for one of the domains  $\Omega_i$ , say i=1, through an equality constraint (13). Here and below also use the scalar products

$$(v, w)_{H_s^s(\partial\Omega_{i,C})} = h_i^{-2s}(v, w)_{\partial\Omega_{i,C}}, \qquad s \in \mathbb{R}$$
(31)

with associated norms

$$\|v\|_{H^{s}(\partial\Omega_{i,C})}^{2} = (v, v)_{H^{s}_{h}(\partial\Omega_{i,C})} = h_{i}^{-2s} \|v\|_{\partial\Omega_{i,C}}^{2}, \qquad s \in \mathbb{R}$$
(32)

These scalar products mimic the corresponding continuous  $H^s(\partial\Omega_{i,C})$  product on the discrete spaces.

### 2.3. Optimality equations

The optimality equations take the form: find  $u_h \in W_h$  such that

$$A(u_h, v) = l(v) \qquad \forall v \in W_h$$
(33)

Here, the forms are defined by

$$A(v, w) = a(v, w) + b(v, w) - c(v, w)$$
(34)

$$a(\boldsymbol{v}, \boldsymbol{w}) = \sum_{i \in I_a} a_i(\boldsymbol{v}_i, \boldsymbol{w}_i)$$
(35)

$$b(\boldsymbol{v}, \boldsymbol{w}) = \sum_{i=1}^{2} b_i(\boldsymbol{v}, \boldsymbol{w})$$
(36)

$$c(\boldsymbol{v}, \boldsymbol{w}) = \sum_{i=1}^{2} c_i(\boldsymbol{v}, \boldsymbol{w})$$
(37)

$$l(\mathbf{v}) = \sum_{i=0}^{2} l_i(\mathbf{v}_i) \tag{38}$$

where

$$b_i(\mathbf{v}, \mathbf{w}) = \gamma_0^{-1} h_i(S_i(\mathbf{v}), DS_i(\mathbf{w}))_{\partial \Omega_i, C}$$

$$\tag{39}$$

with  $S_i$  defined in (23) and

$$DS_i(\mathbf{w}) = \sigma_n(\mathbf{w}_i) - \gamma_0 h_i^{-1} [\mathbf{w}_n]_i$$
 (40)

and

$$c_i(\mathbf{v}, \mathbf{w}) = \gamma_0^{-1} h_i(\sigma_n(\mathbf{v}_i), \sigma_n(\mathbf{w}_i))_{\partial \Omega_i}$$

$$\tag{41}$$

#### 3. Error estimates

#### 3.1. Properties of the forms

• The forms  $a_i$ ,  $i \in I_a$ , are coercive and continuous

$$\|v\|_{V_i}^2 \lesssim a_i(v, v) \qquad v \in V_i \tag{42}$$

$$a_i(\mathbf{v}_i, \mathbf{w}_i) \lesssim \|\mathbf{v}\|_{V_i} \|\mathbf{w}\|_{V_i} \quad \mathbf{v}, \mathbf{w} \in V_i \tag{43}$$

For  $i \in \{1,2\}$ ,  $V_i = H^1(\Omega_i)$  and  $V_0$  will depend on the choice of hybrid model. For a second order model  $V_0 = H^1(\Omega_0)$  and for a fourth order model  $V_0 = H^2(\Omega_0)$ . We define the energy norm

$$\|v\|_a^2 = a(v, v) = \sum_{i \in I} a_i(v_i, v_i)$$
(44)

• The forms  $b_i$  satisfies the monotonicity and continuity

$$\gamma_0^{-1} \|S_i(\mathbf{v}) - S_i(\mathbf{w})\|_{H_{\bullet}^{-1/2}(\partial\Omega_{i,C})}^2 \le b_i(\mathbf{v}, \mathbf{v} - \mathbf{w}) - b_i(\mathbf{w}, \mathbf{v} - \mathbf{w})$$
(45)

$$|b_{i}(\boldsymbol{v},\boldsymbol{r}) - b_{i}(\boldsymbol{w},\boldsymbol{r})| \le \gamma_{0}^{-1} \|S_{i}(\boldsymbol{v}) - S_{i}(\boldsymbol{w})\|_{H_{c}^{-1/2}(\partial\Omega_{i},c)} \|DS_{i}(\boldsymbol{r})\|_{H_{c}^{-1/2}(\partial\Omega_{i},c)}$$

$$(46)$$

with vectorized versions,

$$\sum_{i=1}^{2} \gamma_{0}^{-1} \|S_{i}(\boldsymbol{v}) - S_{i}(\boldsymbol{w})\|_{H_{h}^{-1/2}(\partial\Omega_{i,C})}^{2} \le b(\boldsymbol{v}, \boldsymbol{v} - \boldsymbol{w}) - b(\boldsymbol{w}, \boldsymbol{v} - \boldsymbol{w})$$

$$(47)$$

$$|b(\boldsymbol{v},\boldsymbol{r}) - b(\boldsymbol{w},\boldsymbol{r})| \le \sum_{i=1}^{2} \gamma_0^{-1} \|S_i(\boldsymbol{v}) - S_i(\boldsymbol{w})\|_{H_h^{-1/2}(\partial\Omega_{i,C})} \|DS_i(\boldsymbol{r})\|_{H_h^{-1/2}(\partial\Omega_{i,C})}$$
(48)

See the Appendix for derivations of these inequalities.

• The form c is continuous

$$c(\mathbf{v}, \mathbf{w}) \lesssim \|\mathbf{v}\|_c \|\mathbf{w}\|_c \qquad \mathbf{v}, \mathbf{w} \in W + W_b \tag{49}$$

and we have the inverse bound

$$\|\boldsymbol{v}\|_{c}^{2} = \sum_{i=1}^{2} \gamma_{0}^{-1} \|\sigma_{n}(\boldsymbol{v}_{i})\|_{H_{h}^{-1/2}(\partial\Omega_{i,C})}^{2} \lesssim \sum_{i=1}^{2} \gamma_{0}^{-1} \|\boldsymbol{v}_{i}\|_{V_{i}}^{2} \lesssim \gamma_{0}^{-1} \|\boldsymbol{v}\|_{a}^{2} \qquad \boldsymbol{v} \in W_{h}$$

$$(50)$$

where the last bound follows from (42) for  $i \in \{1,2\}$  and the fact that  $\{1,2\} \subset I_a$ , in both Case 1 and Case 2.

### 3.2. Estimates

**Proposition 3.1.** The discrete problem (33) admits a unique solution  $u_h \in W_h$  such that

$$\|\boldsymbol{u}_{h}\|_{a}^{2} + \sum_{i=1}^{2} \gamma_{0}^{-1} \|S_{i}(\boldsymbol{u}_{h}) - S_{i}(\boldsymbol{0})\|_{H_{h}^{-1/2}(\partial\Omega_{i,C})}^{2} \lesssim \sum_{i \in I_{a}} \|\boldsymbol{f}_{i}\|_{V_{i}^{*}}^{2} + \sum_{i=1}^{2} \gamma_{0}^{-1} h \|S_{i}(\boldsymbol{0})\|_{\partial\Omega_{i,C}}^{2}$$

$$(51)$$

Proof. We have

$$l(\mathbf{v}) = A(\mathbf{v}, \mathbf{v}) = \|\mathbf{v}\|_{\alpha}^{2} + b(\mathbf{v}, \mathbf{v}) - \|\mathbf{v}\|_{\alpha}^{2}$$
(52)

where

$$b(\mathbf{v}, \mathbf{v}) = b(\mathbf{v}, \mathbf{v} - \mathbf{0}) - b(\mathbf{0}, \mathbf{v} - \mathbf{0}) + b(\mathbf{0}, \mathbf{v})$$
(53)

and thus

$$||v||_{a}^{2} - ||v||_{c}^{2} + b(v, v - 0) - b(0, v - 0) = l(v) - b(0, v) \le |l(v)| + |b(0, v)|$$

$$(54)$$

Here we have using (50), for  $\gamma_0$  large enough,

$$\|v\|_{a}^{2} - \|v\|_{a}^{2} \ge \|v\|_{a}^{2} - C_{1}\gamma_{a}^{-1}\|v\|_{a}^{2} \ge (1 - C_{1}\gamma_{a}^{-1})\|v\|_{a}^{2} \ge C_{2}\|v\|_{a}^{2}$$

$$(55)$$

with  $C_2 > 0$  and by (47),

$$b(\boldsymbol{v}, \boldsymbol{v} - \boldsymbol{0}) - b(\boldsymbol{0}, \boldsymbol{v} - \boldsymbol{0}) \ge \sum_{i=1}^{2} \gamma_0^{-1} \|S_i(\boldsymbol{v}_i) - S_i(\boldsymbol{0})\|_{H_h^{-1/2}(\partial\Omega_{i,C})}^2$$
(56)

We thus have

$$C_2 \|\boldsymbol{v}\|_a^2 + \sum_{i=1}^2 \gamma_0^{-1} \|S_i(\boldsymbol{v}_i) - S_i(\boldsymbol{0})\|_{H_b^{-1/2}(\partial\Omega_iC)}^2 \le |l(\boldsymbol{v})| + |b(\boldsymbol{0}, \boldsymbol{v})|$$
(57)

Next, estimating the right hand side, we have

$$|l(v)| \lesssim ||f||_{W^*} ||v||_{W} \lesssim ||f||_{W^*} ||v||_{a}$$
 (58)

and

$$|b(\mathbf{0}, \mathbf{v})| \le \sum_{i=1}^{2} \gamma_0^{-1} ||S_i(\mathbf{0})||_{H_h^{-1/2}(\partial \Omega_{i,C})} ||DS_i(\mathbf{v})||_{H_h^{-1/2}(\partial \Omega_{i,C})}^2$$
(59)

$$= \sum_{i=1}^{2} \gamma_0^{-1} \|S_i(\mathbf{0})\|_{H_h^{-1/2}(\partial\Omega_{i,C})} \|S_i(\mathbf{v}) - S_i(\mathbf{0})\|_{H_h^{-1/2}(\partial\Omega_{i,C})}^2$$
(60)

$$\leq \sum_{i=1}^{2} \frac{1}{2} \gamma_0^{-1} \|S_i(\mathbf{0})\|_{H_h^{-1/2}(\partial \Omega_{i,C})}^2 + \frac{1}{2} \gamma_0^{-1} \|S_i(\mathbf{v}) - S_i(\mathbf{0})\|_{H_h^{-1/2}(\partial \Omega_{i,C})}^2$$

$$(61)$$

where we used the identity  $S_i(v) = S_i(0) + DS_i(v)$ , which holds for affine maps. Using kick-back for the second term in (61) these estimates prove the desired stability estimate. Using the Brouwer fixed point theorem, we can prove that there exists a solution; see [36] for details. Uniqueness follows from the stability estimate.

**Theorem 3.1.** The solution  $u_h \in W_h$  to (33) satisfies the following best approximation estimate

$$\|\mathbf{u} - \mathbf{u}_h\|_a^2 + \sum_{i=1}^2 \gamma_0^{-1} \|S_i(\mathbf{u}) - S_i(\mathbf{u}_h)\|_{H_h^{-1/2}(\partial\Omega_{i,C})}^2$$
(62)

$$\lesssim \inf_{\boldsymbol{v}_h \in W_h} \left( (1 + \gamma_0^{-1}) \|\boldsymbol{u} - \boldsymbol{v}_h\|_a^2 + \sum_{i=1}^2 \gamma_0^{-1} \|\sigma_n(\boldsymbol{u}_i - \boldsymbol{v}_{h,i})\|_{H_h^{-1/2}(\partial\Omega_{i,C})}^2 + \gamma_0 \|[\boldsymbol{u} - \boldsymbol{v}_h]_i\|_{H_h^{1/2}(\partial\Omega_{i,C})}^2 \right)$$

$$(63)$$

**Proof.** We first note that we have the Galerkin orthogonality

$$a(\mathbf{u} - \mathbf{u}_h, \mathbf{v}) + b(\mathbf{u}, \mathbf{v}) - b(\mathbf{u}_h, \mathbf{v}) - c(\mathbf{u} - \mathbf{u}_h, \mathbf{v}) = 0, \quad \forall \mathbf{v} \in W_h$$
 (64)

Next, we split the error,  $e = u - u_h$ , in an approximation error  $\theta$  and a discrete error  $e_h \in W_h$ ,

$$e := u - u_h = (u - v_h) + (v_h - u_h) = \theta + e_h, \quad v_h \in W_h$$
 (65)

Using the coercivity (44) of a, monotonicity (47) of b, followed by Galerkin orthogonality (64), we get

$$\|e\|_a^2 + \sum_{i=1}^2 \gamma_0^{-1} \|S_i(u) - S_i(u_h)\|_{H_h^{-1/2}(\partial\Omega_{i,C})}^2$$
(66)

$$\leq a(e,e) + b(u,e) - b(u_h,e) \tag{67}$$

$$= a(\mathbf{e}, \boldsymbol{\theta}) + b(\mathbf{u}, \boldsymbol{\theta}) - b(\mathbf{u}_h, \boldsymbol{\theta}) + \underbrace{a(\mathbf{e}, \mathbf{e}_h) + b(\mathbf{u}, \mathbf{e}_h) - b(\mathbf{u}_h, \mathbf{e}_h)}_{=c(\mathbf{e}, \mathbf{e}_h)}$$

$$(68)$$

$$= a(e,\theta) + b(u,\theta) - b(u_h,\theta) + c(e,e_h)$$
(69)

$$\leq \|\boldsymbol{e}\|_{a} \|\boldsymbol{\theta}\|_{a} + \sum_{i=1}^{2} \gamma_{0}^{-1} \|S_{i}(\boldsymbol{u}) - S_{i}(\boldsymbol{u}_{h})\|_{H_{h}^{-1/2}(\partial\Omega_{i,C})} \|DS_{i}(\boldsymbol{\theta})\|_{H_{h}^{-1/2}(\partial\Omega_{i,C})} + \frac{1}{2} \|\boldsymbol{\theta}\|_{c}^{2} + \frac{3}{2} C \gamma_{0}^{-1} \|\boldsymbol{\theta}\|_{a}^{2} + \frac{3}{2} C \gamma_{0}^{-1} \|\boldsymbol{e}\|_{a}^{2}$$

$$(70)$$

In (70) we used the continuity of a and b, and the estimate

$$c(\mathbf{e}, \mathbf{e}_h) = c(\mathbf{\theta}, \mathbf{e}_h) + c(\mathbf{e}_h, \mathbf{e}_h) \tag{71}$$

$$\leq \|\theta\|_{c} \|e_{h}\|_{c} + \|e_{h}\|_{c}^{2} \tag{72}$$

$$\leq \frac{1}{2} \|\boldsymbol{\theta}\|_{c}^{2} + \frac{3}{2} \|\boldsymbol{e}_{h}\|_{c}^{2} \tag{73}$$

$$\leq \frac{1}{2} \|\theta\|_{c}^{2} + \frac{3}{2} C \gamma_{0}^{-1} \|e_{h}\|_{a}^{2} \tag{74}$$

$$\leq \frac{1}{2} \|\theta\|_{c}^{2} + \frac{3}{2} C \gamma_{0}^{-1} \|\theta\|_{a}^{2} + \frac{3}{2} C \gamma_{0}^{-1} \|e\|_{a}^{2} \tag{75}$$

where we used the inverse estimate (50). Splitting the first and second terms in (70) using  $ab \le a^2/2 + b^2/2$  and taking  $\gamma_0$  large enough, we may use a kick-back argument to get

$$\|e\|_a^2 + \sum_{i=1}^2 \gamma_0^{-1} \|S_i(u) - S_i(u_h)\|_{H_b^{-1/2}(\partial\Omega_{i,C})}^2$$
(76)

where we used the triangle inequality to conclude that

$$\gamma_0^{-1} \|DS_i(\mathbf{v})\|_{H^{-1/2}(\partial\Omega_{i,C})}^2 = \gamma_0^{-1} h \|\sigma_n(\mathbf{v}_i) - \gamma_0 h^{-1}[\mathbf{v}_n]_i\|_{\partial\Omega_{i,C}}^2$$
(79)

$$\leq \gamma_0^{-1} h \|\sigma_n(v_i)\|_{\partial \Omega_{r,0}}^2 + \gamma_0 h^{-1} \|[v_n]_i\|_{\partial \Omega_{r,0}}^2 \tag{80}$$

$$= \gamma_0^{-1} \|\sigma_n(v_i)\|_{H_i^{-1/2}(\partial\Omega_iC)}^2 + \gamma_0 \|[v_n]_i\|_{H_i^{1/2}(\partial\Omega_iC)}^2$$
(81)

Thus, the proof is complete.  $\square$ 

**Remark 3.1.** Letting  $\mathcal{T}_h(\partial\Omega_{i,C})$  denote the elements in  $\mathcal{T}_{h,i}$  with a face that intersects  $\partial\Omega_{i,C}$  and using the element-wise trace inequality  $\|w\|_{\partial T}^2 \lesssim h^{-1} \|w\|_T^2 + h\|\nabla w\|_T^2$  for  $w \in H^1(T)$ , we obtain

$$\gamma_0^{-1} h_i \|\sigma_n(v_i)\|_{\partial\Omega_{iC}}^2 + \gamma_0 h_i^{-1} \|[v_n]_i\|_{\partial\Omega_{iC}}^2$$
(82)

Setting  $v = \theta = u - v_h$ , and taking  $v_h$  to an interpolant  $\pi_h u$  of the exact solution u that satisfies optimal order interpolation error bounds (19), we conclude that our best approximation result, indeed leads to the optimal order energy error estimate,

$$\|\boldsymbol{u} - \boldsymbol{u}_h\|_a^2 + \sum_{i=1}^2 \gamma_0^{-1} \|S_i(\boldsymbol{u}) - S_i(\boldsymbol{u}_h)\|_{H_h^{-1/2}(\partial\Omega_{i,C})}^2 \lesssim \begin{cases} \sum_{i=1}^2 h_0^{2p_0+1}(h_0/h_i) + \sum_{i=1}^2 h_i^{2p_i} & \text{Case 1} \\ h_0^{2(p_0+1-s_0)} + \sum_{i=1}^2 h_0^{2p_0+1}(h_0/h_i) + \sum_{i=1}^2 h^{2p_i} & \text{Case 2} \end{cases}$$
(85)

Here, in Case 2,  $a_0$  is a form defined on  $H^{s_0}(\Omega_0)$  and we assume that  $V_{h,0} \subset H^{s_0}(\Omega_0)$ . In Case 1 when  $a_0$  is not present the estimate simplifies. For both cases we can take piecewise constants in  $V_{0,h}$  and still get convergence, see the numerical example Section 4.1.1. Note that we can take  $h_0$  arbitrarily small compared to  $h_i$ , but not the other way around.

## 4. Numerical examples

One domain is fixed using Dirichlet boundary conditions in the numerical examples presented below. To remove the rigid body motions of the other, we use scalar Lagrange multipliers to ensure that the mean horizontal displacements are zero. We emphasize that our interface variable can be vector valued  $(u_0)$  or scalar  $(n \cdot u_0)$  depending on the problem type. We comment on this below.

### 4.1. A 2D Hertz problem

### 4.1.1. Comparison to the standard Nitsche method

In this Section, we study how the discretization of the interface (without interface model) compares to a standard Nitsche method as given in [10]. In doing this, we tie the interface variable to the surface of one of the bodies. It is then clear that the discretization of the bodies determines the error of the computation in the limit of fine discretization of the interface variable, as the interface variables cannot improve the accuracy of the discretization of the surface of the body to which it is tied. Here the interface variable is a scalar, approximating the normal displacement.

We consider a half-cylinder in contact with a rectangular block. The domains, load and boundary conditions are given in Fig. 3; the meshes used are given in Fig. 4. These meshes are fixed using the computations: 19 600 bilinear elements for the block and 30 752 linear triangular elements for the half cylinder. The block is fixed vertically at its bottom boundary and horizontally at (x, y) = (0, -1). The half-cylinder  $(\Omega_1)$  is loaded by a line load f = (0, -50) at y = 1 and has elastic moduli  $E_1 = 7000$  and  $v_1 = 0.3$ . It is meshed using  $P^1$  triangles. The block  $(\Omega_2)$  has elastic moduli  $E_2 = 4000$ ,  $v_2 = 0.3$  and is discretized using  $Q_1$  elements. We assume plane strain so that  $\lambda_i = v_i E_i/((1 + v_i)(1 - 2v_i))$  and  $\mu_i = E_i/(2(1 + v_i))$ , and we set  $\gamma_i = 10(\lambda_i + \mu_i)$ . For the approximation of  $n \cdot u_0$  we use three different choices: equidistributed piecewise constants, equidistributed linear continuous elements, and equidistributed quadratic continuous elements, on

$$\Omega_0 := \{ x \in [-0.4, 0.4], y = 0 \}$$
 (86)

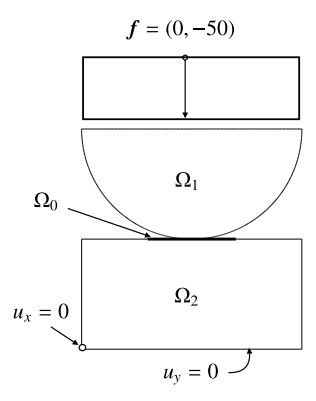


Fig. 3. Domains, load and boundary conditions used for the Hertz problem.

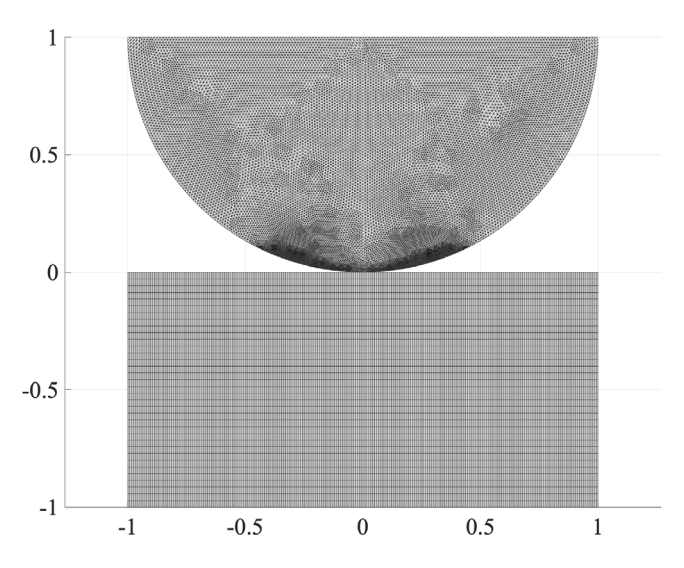


Fig. 4. Meshes used for the Hertz problem.

These approximations are tied to the upper boundary of the block by an equality constraint. In Fig. 5 we show the solution obtained with Nitsche's original method compared with the corresponding Hertz solution for two cylinders in contact, the upper with radius r = 1 and the lower with  $r = \infty$  (cf., e.g., [37]). This is not identical to the setup in the problem we solve but indicates the accuracy of the solution. In Fig. 6 we compare the different approximation of the interface variable and compare the error to that of the standard Nitsche method. With  $p = n_1 \cdot \sigma_1 \cdot n_1$  and  $p_h$  its discrete counterpart, we define the pressure error as

$$e_p = \frac{\|p - p_h\|_{L_2}}{\|p\|_{L_2}} \tag{87}$$

We start by dividing  $\Omega_0$  into two elements and then successively double the number of elements on the interface. We see that the quadratic approximation needs about 16 elements to achieve the expected accuracy, the linear about 64 elements, whereas the piecewise constant approximation needs more than 2048 (last data point). The number of surface elements on  $\Omega_2$  coinciding with  $\Omega_0$  equals 224. Thus, with a good approximation of the interface variable, not many elements are needed to regain the accuracy of the original Nitsche method in this case.

### 4.1.2. Contact zones and pressures

In this Section, we show how the different methods act in the contact zone, and what pressure distributions they give. We show the case of  $\log(h_0) \approx -5.07$ , corresponding to 128 elements for the approximation of  $n \cdot u_0$  (cf. Fig. 6 for errors). In Fig. 7 we show a zoom of the edge of the contact zone, and in Fig. 8 we show the corresponding computed pressure. We note that the sources of the error are the spikes in pressure caused by the jumps in the discretization of  $n \cdot u_0$ . In Figs. 9–12 we show contact zones and pressures for linear and quadratic approximations of  $n \cdot u_0$ . At this discretization, they are close, but for coarser discretizations, the kinks in the linear approximation will lead to a larger error than in the quadratic approximation, as seen in Fig. 6.

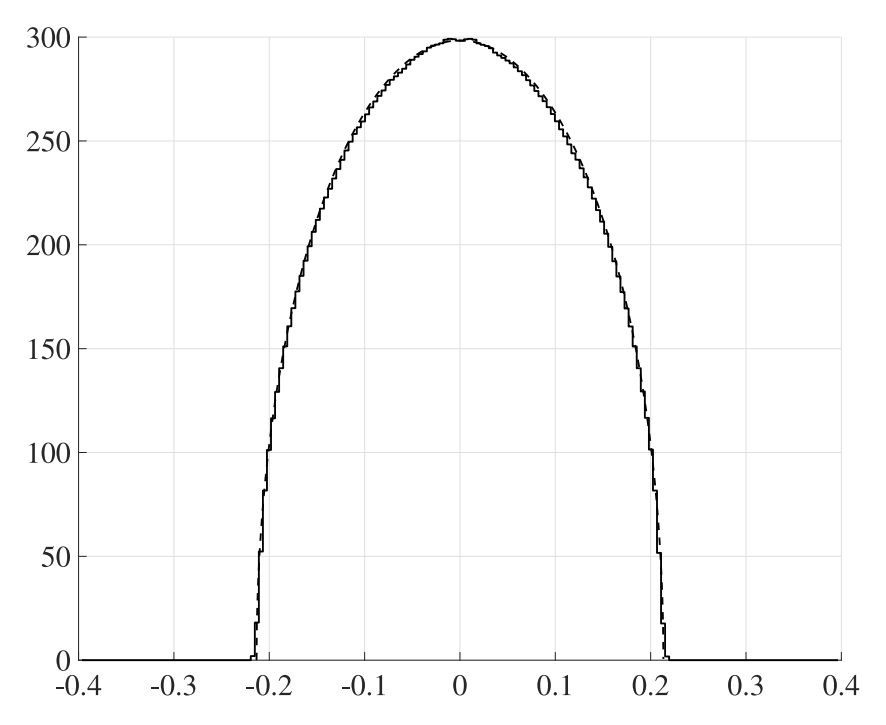


Fig. 5. Exact (dashed line) and computed pressures with the original Nitsche method.

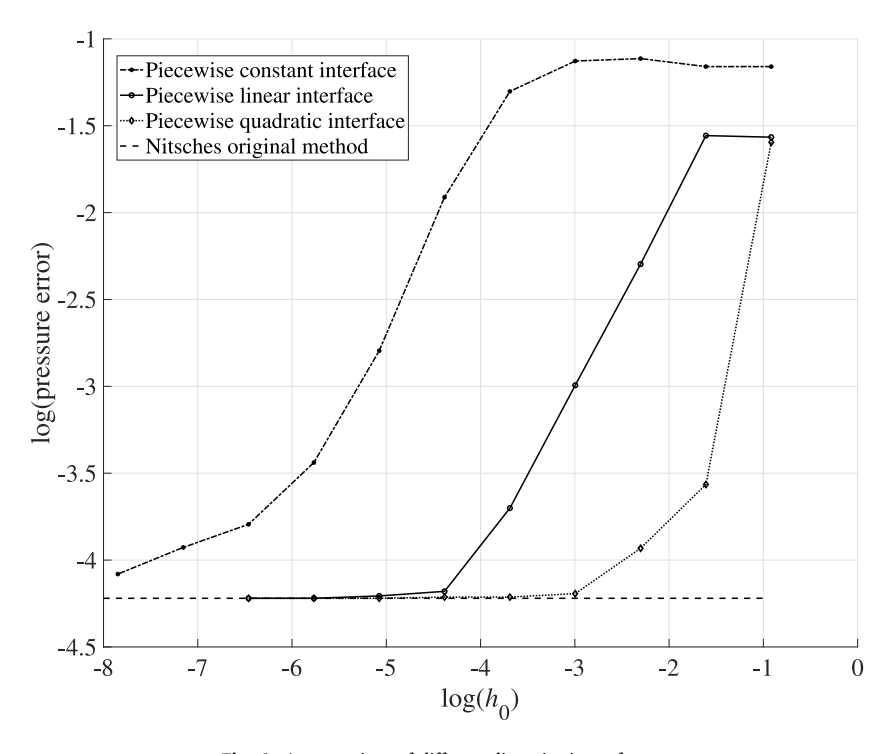


Fig. 6. A comparison of different discretizations of  $n \cdot u_0$ .

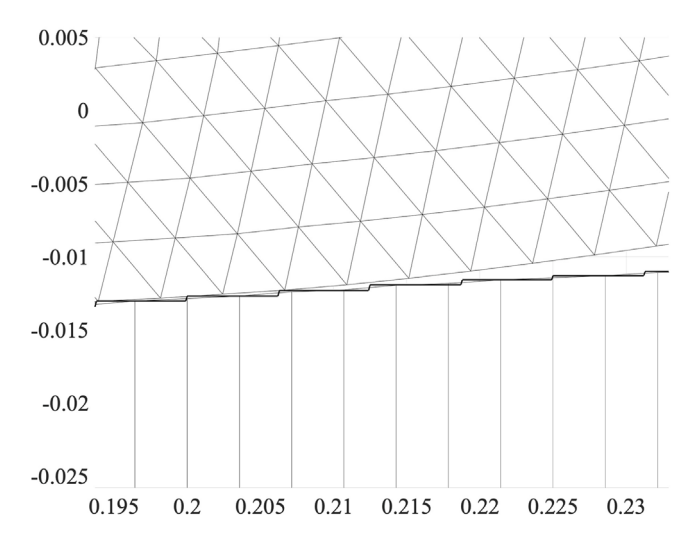


Fig. 7. Zoom of the contact zone for piecewise constant  $n \cdot u_0$ .

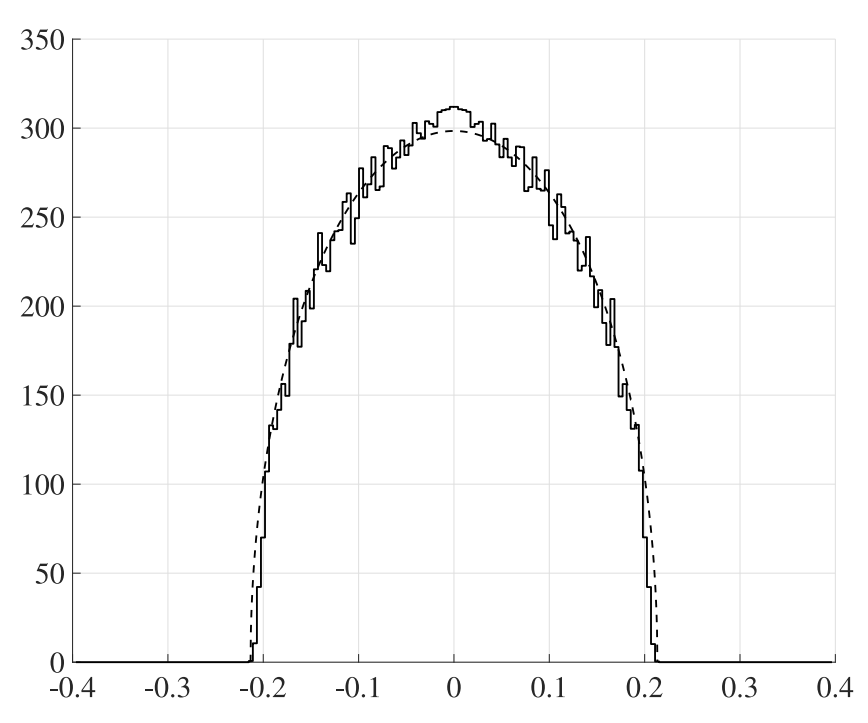


Fig. 8. Contact pressure for piecewise constant  $n \cdot u_0$ .

### 4.2. Contact problems with model coupling

In this section, we focus on the qualitative behavior of our models, as no exact solutions are known.

### 4.2.1. The plate model

In this example, we use a plate model to calculate the hybrid variable. We consider the Kirchhoff plate model, posed on a rectangular domain  $\Omega_0$ , in the (x,y)-plane, where we seek an out-of-plane (scalar) displacement  $u_0$ , with  $u_0=(0,0,u_0)$ , to which we associate the strain (curvature) tensor

$$\epsilon_p(\nabla u_0) := \frac{1}{2} \left( \nabla \otimes (\nabla u_0) + (\nabla u_0) \otimes \nabla \right) = \nabla \otimes \nabla u_0 = \nabla^2 u_0 \tag{88}$$

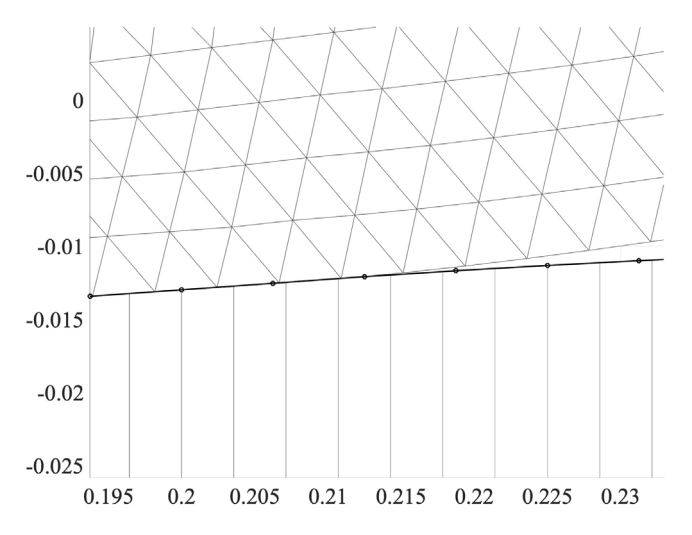


Fig. 9. Zoom of the contact zone for piecewise linear  $n \cdot u_0$ .

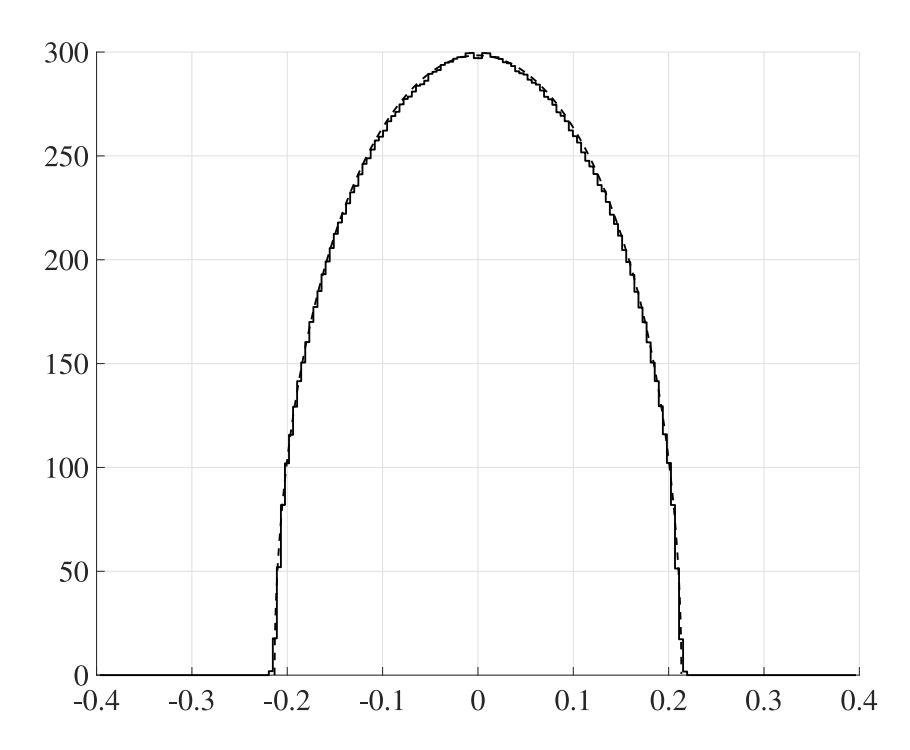


Fig. 10. Contact pressure for piecewise linear  $\mathbf{n} \cdot \mathbf{u}_0$ .

and the plate stress (moment) tensor

$$\sigma_{p}(\nabla u_{0}) := D\left(\epsilon(\nabla u_{0}) + \nu(1 - \nu_{0})^{-1} \operatorname{div} \nabla u_{0} \boldsymbol{I}\right)$$
(89)

$$=D\left(\nabla^{2}u_{0}+\nu(1-\nu_{0})^{-1}\Delta u_{0}I\right)$$
(90)

where

$$D := \frac{E_0 t^3}{12(1 + \nu_0)} \tag{91}$$

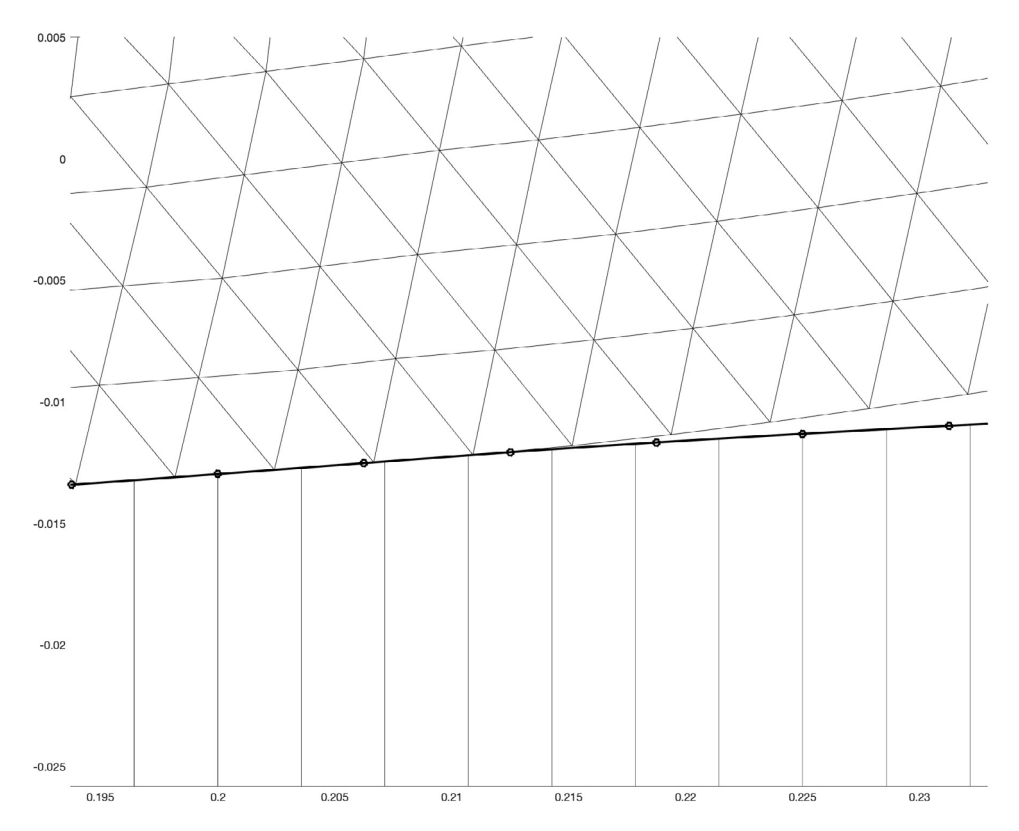


Fig. 11. Zoom of the contact zone for piecewise quadratic  $n \cdot u_0$ .

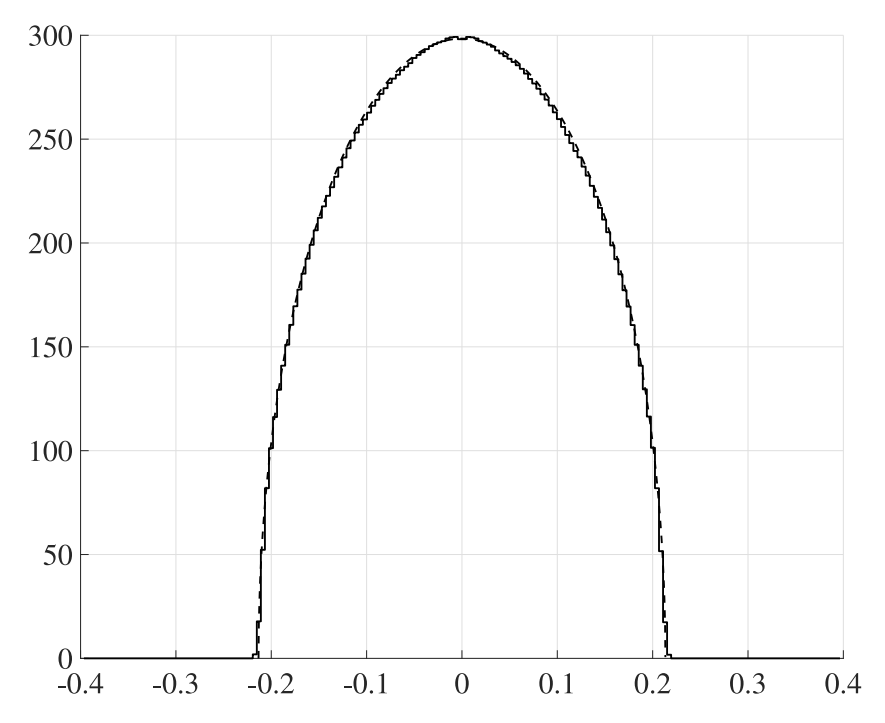


Fig. 12. Contact pressure for piecewise quadratic  $n \cdot u_0$ .

with  $E_0$  the Young's modulus,  $v_0$  the Poisson's ratio, and t the plate thickness. The equilibrium equations of a free Kirchhoff plate take the form

$$\operatorname{div}\operatorname{div}\sigma_{n}(\nabla u_{0})=0 \qquad \text{in } \Omega_{0} \tag{92}$$

where **div** and div denote the divergence of a tensor and a vector field, respectively. Multiplying by v and integrating by parts, the form  $a_0(\cdot, \cdot)$  is found as

$$a_0(u_0, v) := (\sigma_n(\nabla u_0), \epsilon_n(\nabla v))_{\Omega_0} \tag{93}$$

We consider a problem consisting of  $\Omega_1$  being a stiff ball of radius r=1,  $\Omega_2$  a block of dimensions  $(-2.5, 2.5) \times (-2.5, 2.5) \times (-1, 0)$ , and  $\Omega_0$  a plate resting on the block. Fig. 13 shows the configuration and meshes used. The ball has constitutive parameters  $E_1=20\,000$ ,  $v_1=0.33$ , the block has  $E_2=25$ , v=0.33, and the plate has  $E_0=1000$ , t=0.1, and v=0.5. The ball is being pushed downwards by a volume force  $f_1=(0,0,-10)$ . We take  $\gamma_i=100E_i$ . The block and the ball are discretized using  $P^1$  tetrahedral elements, and the plate is discretized using Bogner–Fox–Schmit elements [38], which is basically the outer product of cubic splines with some degrees of freedom removed, The reason for choosing this element is that it is very simple to implement on rectangular grids. Dirichlet boundary conditions  $u_2=0$  are applied to the block at the bottom and at the sides.

In Fig. 14 we show the initial configuration; in Fig. 15, we show the deformation of the whole configuration; in Fig. 16, we show the deformation of the plate and the block.

#### 4.2.2. The membrane model

In what follows,  $\Gamma := \Omega_0$  denotes a closed and oriented surface, for simplicity without boundary, which is embedded in  $\mathbb{R}^3$  and equipped with exterior normal  $n_\Gamma$ . The membrane is assumed to occupy the domain  $\Omega_t = \Gamma \times (-t/2, t/2)$  with t the thickness of the membrane, assumed constant for simplicity. We let  $\rho$  denote the signed distance function fulfilling  $\nabla \rho|_{\Gamma} = n_{\Gamma}$ .

For a given function  $u: \Gamma \to \mathbb{R}$ , we assume that there exists an extension  $\bar{u}$ , in some neighborhood of  $\Gamma$ , such that  $\bar{u}|_{\Gamma} = u$ . The tangent gradient  $\nabla_{\Gamma}$  on  $\Gamma$  can be defined by

$$\nabla_{\Gamma} u = P_{\Gamma} \nabla \overline{u} \tag{94}$$

with  $\nabla$  the  $\mathbb{R}^3$  gradient and  $P_{\Gamma} = P_{\Gamma}(x)$  the orthogonal projection of  $\mathbb{R}^3$  onto the tangent plane of  $\Gamma$  at  $x \in \Gamma$  given by

$$P_{\Gamma} = I - n_{\Gamma} \otimes n_{\Gamma} \tag{95}$$

where I is the identity matrix. The tangent gradient defined by (94) is easily shown to be independent of the extension  $\bar{u}$ . In the following, we shall not distinguish between functions on  $\Gamma$  and their extensions when defining differential operators.

The surface gradient has three components, which we shall denote by

$$\nabla_{\Gamma} u =: \left( \frac{\partial u}{\partial x^{\Gamma}}, \frac{\partial u}{\partial y^{\Gamma}}, \frac{\partial u}{\partial z^{\Gamma}} \right) \tag{96}$$

For a vector-valued function v(x), we define the tangential Jacobian matrix as the transpose of the outer product of  $\nabla_{\Gamma}$  and v,

$$(\nabla_{\Gamma} \otimes \boldsymbol{\nu})^{\mathrm{T}} := \begin{bmatrix} \frac{\partial v_{1}}{\partial x^{\Gamma}} & \frac{\partial v_{1}}{\partial y^{\Gamma}} & \frac{\partial v_{1}}{\partial z^{\Gamma}} \\ \frac{\partial v_{2}}{\partial x^{\Gamma}} & \frac{\partial v_{2}}{\partial y^{\Gamma}} & \frac{\partial v_{2}}{\partial z^{\Gamma}} \\ \frac{\partial v_{3}}{\partial x^{\Gamma}} & \frac{\partial v_{3}}{\partial y^{\Gamma}} & \frac{\partial v_{3}}{\partial z^{\Gamma}} \end{bmatrix},$$
 (97)

the surface divergence  $\nabla_{\Gamma} \cdot \boldsymbol{v} := \operatorname{tr} \nabla_{\Gamma} \otimes \boldsymbol{v}$ , and the in-plane strain tensor

$$\epsilon_{\Gamma}(\mathbf{u}) := P_{\Gamma} \epsilon(\mathbf{u}) P_{\Gamma}, \quad \text{where} \quad \epsilon(\mathbf{u}) := \frac{1}{2} \left( \nabla \otimes \mathbf{u} + (\nabla \otimes \mathbf{u})^{\mathrm{T}} \right)$$
 (98)

is the 3D strain tensor. The corresponding stress tensor is given by

$$\sigma_{\Gamma} = 2\mu_{\Gamma}\epsilon_{\Gamma} + \lambda_{\Gamma} \operatorname{tr}\epsilon_{\Gamma} P_{\Gamma} \tag{99}$$

where, with Young's modulus  $E_{\Gamma}$  and Poisson's ratio  $v_{\Gamma}$ ,

$$\mu_{\Gamma} = \frac{E_{\Gamma}t}{2(1+\nu_{\Gamma})}, \quad \lambda_{\Gamma} = \frac{E_{\Gamma}\nu_{\Gamma}t}{1-\nu_{\Gamma}^2} \tag{100}$$

are the Lamé parameters in plane stress (multiplied by the thickness).

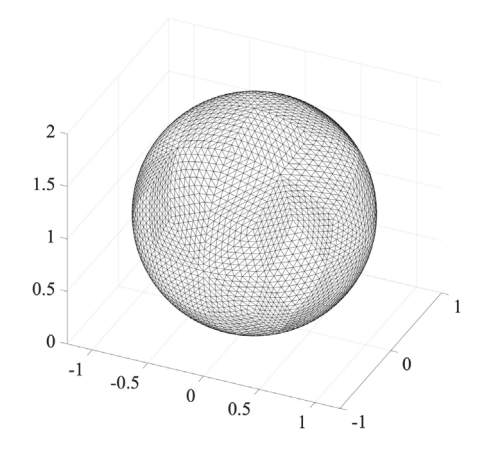
The equilibrium equations on an unloaded membrane are given by (cf. [39])

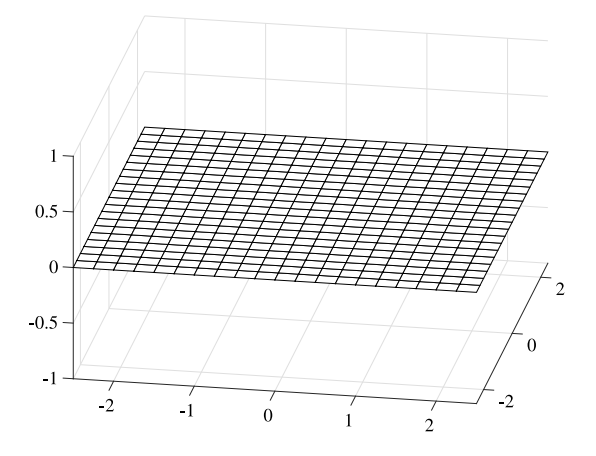
$$-\nabla_{\Gamma} \cdot \sigma_{\Gamma}(u_0) = 0 \quad \text{on } \Gamma, \tag{101}$$

By multiplying the equilibrium equation by  $v_0$  and integrating by parts, we find the form  $a_0(\cdot,\cdot)$  as

$$a_0(\mathbf{u}_0, \mathbf{v}_0) = (2\mu_{\Gamma} \epsilon_{\Gamma}(\mathbf{u}_0), \epsilon_{\Gamma}(\mathbf{v}_0))_{\Gamma} + (\lambda_{\Gamma} \nabla_{\Gamma} \cdot \mathbf{u}_0, \nabla_{\Gamma} \cdot \mathbf{v}_0)_{\Gamma}$$

$$(102)$$





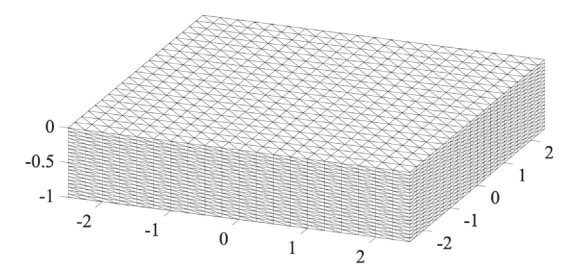


Fig. 13. Geometry and meshes used for the plate contact problem.

In this case, the interface variable is thus a vector-valued function.

We consider a problem with  $\Omega_1$  a ball and  $\Omega_2$  a block of the same dimensions as in the previous Section. The ball and block have fixed constitutive parameters  $E_1=1000$ ,  $v_1=0.33$  and  $E_2=100$ ,  $v_2=0.3$ . The ball is covered by a membrane with t=0.1 and  $v_{\Gamma}=0.5$ , whose Young's modulus we vary to show its stiffening effect. The discretization of the ball and the block are as in the previous section, and we let the surface mesh of the ball serve as a  $P^1$  mesh for the membrane. We use  $\gamma_i=100E_i$ . The ball is again loaded with a volume load  $f_2=(0,0,-10)$ .

In Fig. 17, we show the deformations and normal stress on the ball surface when the membrane has zero stiffness (acts as a standard hybrid variable), in Fig. 18, we show the deformations and normal stress on the ball surface when  $E_{\Gamma} = 2000$ , and, finally, in Fig. 19 when  $E_{\Gamma} = 20000$ . The stiffening effect is clearly visible. Note that, counterintuitively, the maximum normal stress on the ball surface decreases as the membrane stiffens, even though the contact zone decreases. This is due to the membrane equilibrating

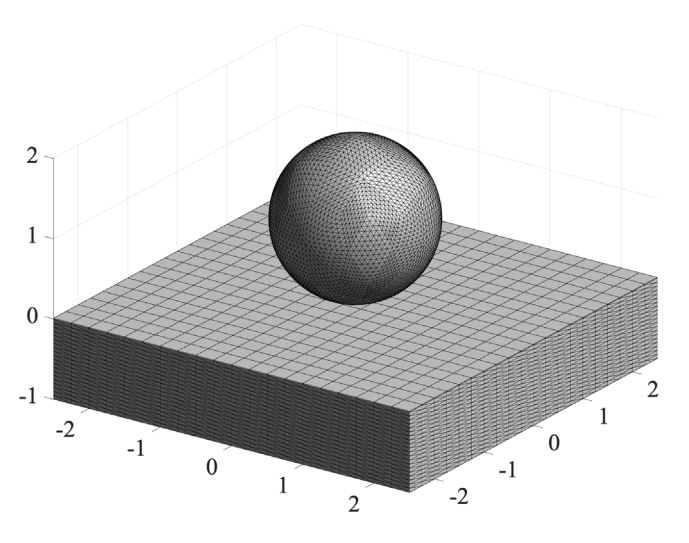


Fig. 14. Initial configuration.

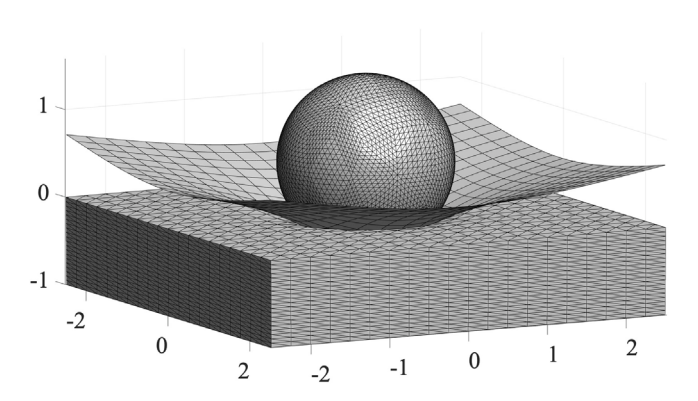


Fig. 15. Deformation of the configuration.

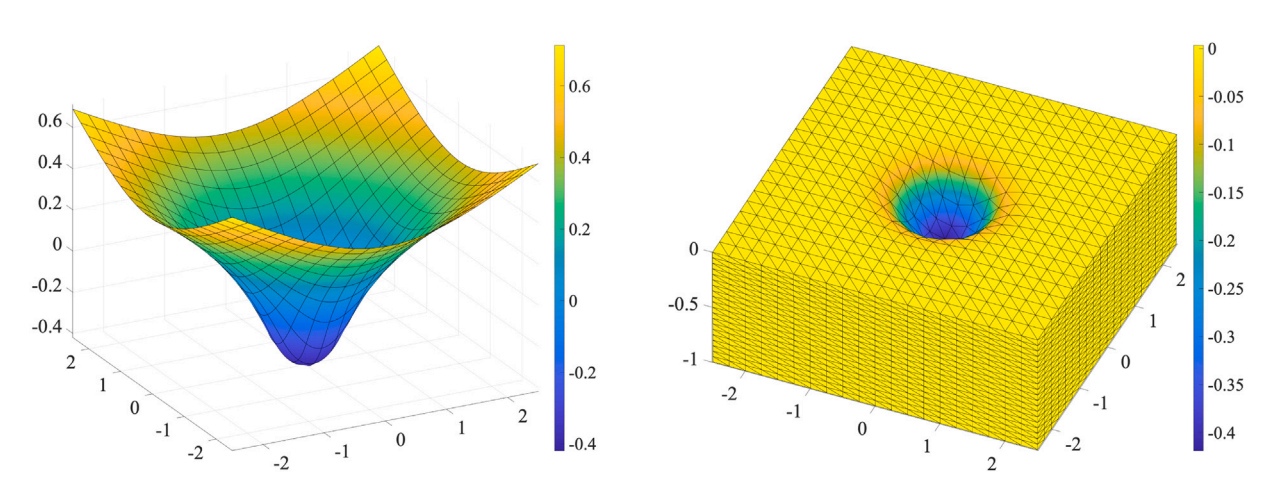
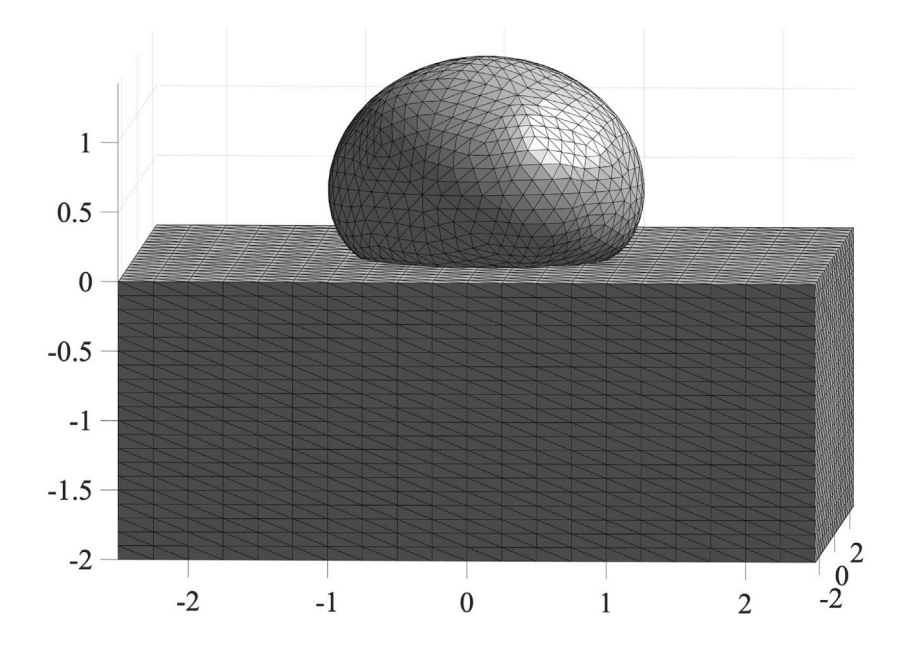


Fig. 16. Deformation of the plate and the block.



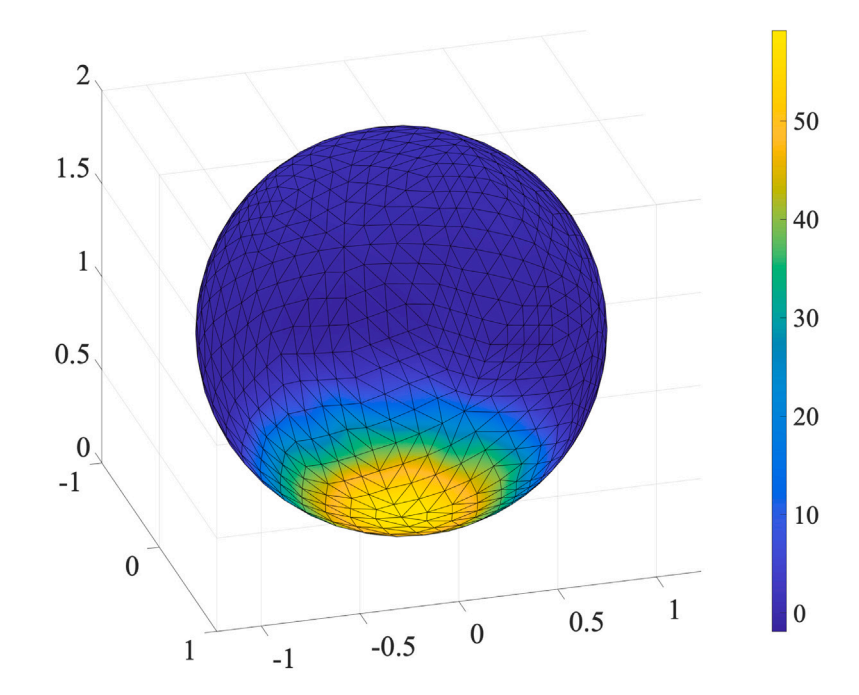


Fig. 17. Deformations and normal stress on the ball surface with zero stiffness of the membrane.

the stresses over the ball more effectively as it stiffens. The stresses shown have been  $L_2$ -projected from the piecewise constant stresses onto  $V_{h,1}$ .

### 5. Conclusions

In this work, we have developed a novel augmented Lagrangian framework for modeling friction-free contact between two elastic bodies. The core of our approach is a Nitsche-based method with a hybrid displacement variable defined on an interstitial layer. This formulation introduces significant flexibility by decoupling the computational domains, allowing the bodies in contact to interact

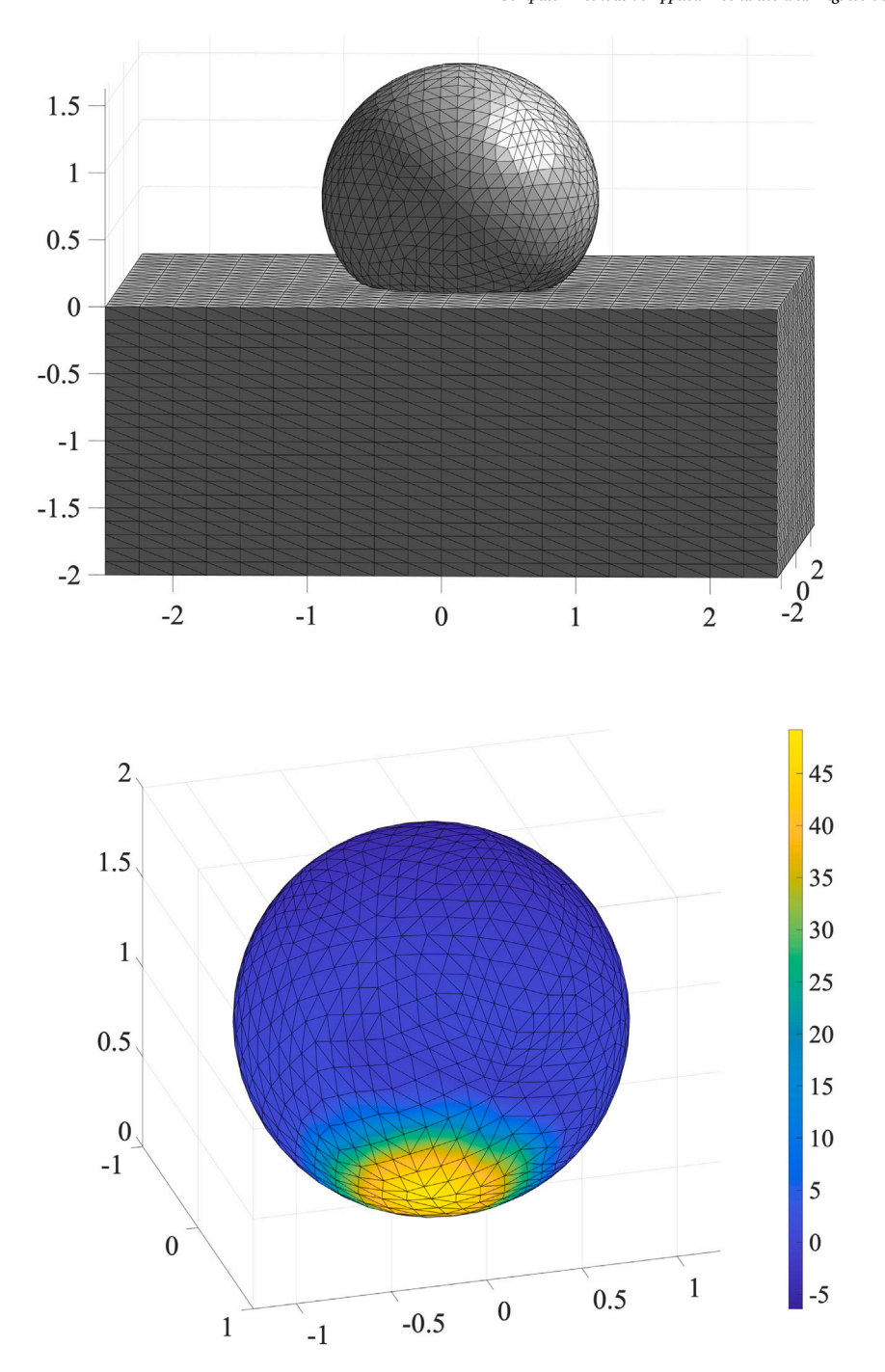


Fig. 18. Deformations and normal stress on the ball surface with  $E_{\Gamma}=2000$ .

exclusively through the layer. The independent approximation of the layer avoids challenges associated with the intersection of unrelated meshes and opens possibilities for additional modeling, such as incorporating a membrane or other interface effects.

We demonstrated the stability and accuracy of the method by proving stability estimates and deriving error bounds. These theoretical results underline the robustness and convergence of the approach, making it suitable for complex contact problems where traditional methods may face limitations.

Moreover, the hybrid variable approach offers a natural framework for incorporating additional physical phenomena or constraints at the interface, such as thin structures or surface layers, without altering the underlying contact model. This adaptability enhances the potential applicability of the method to a wide range of problems in computational mechanics.

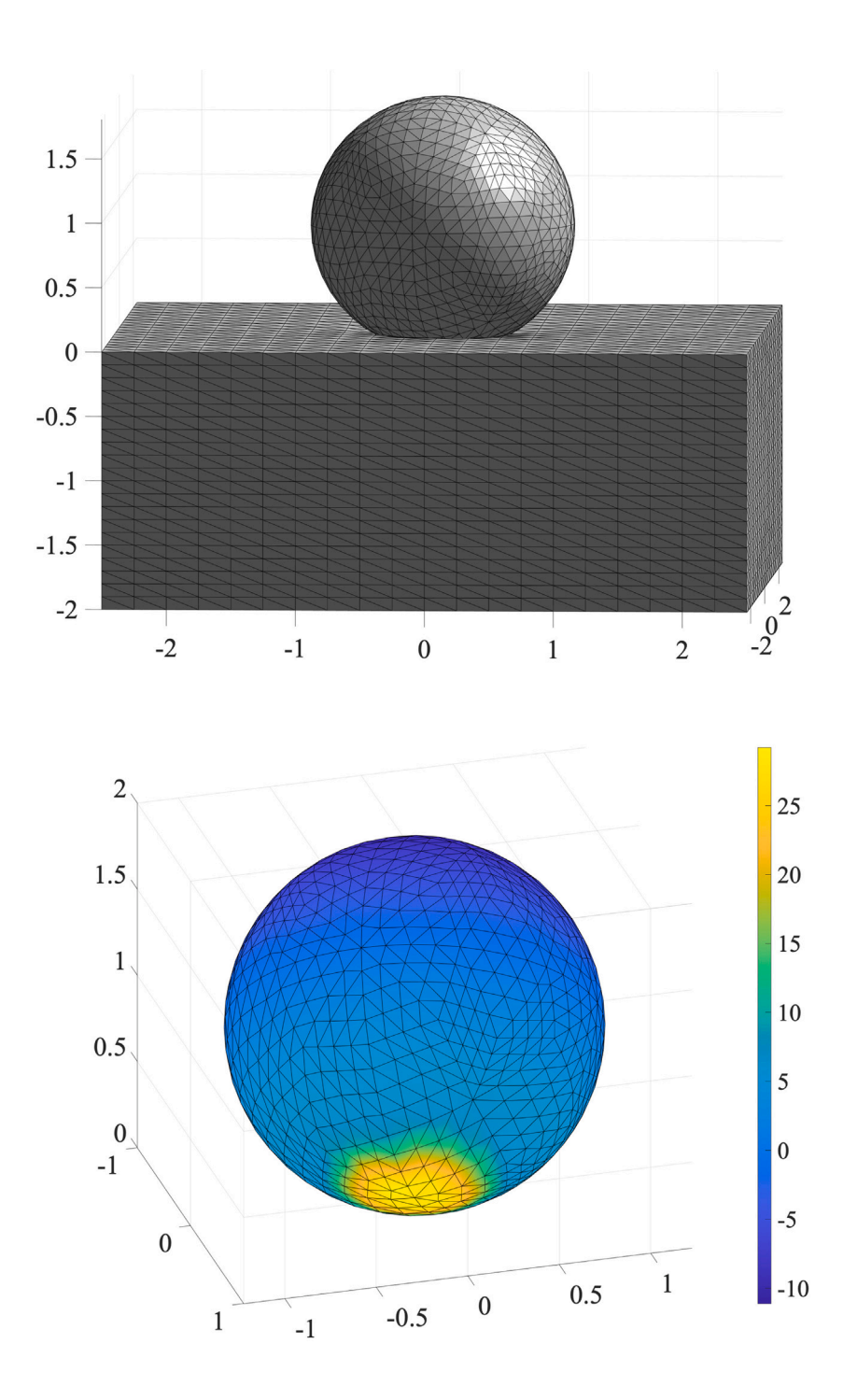


Fig. 19. Deformations and normal stress on the ball surface with  $E_{\Gamma}=20000$ .

The numerical examples illustrate the proposed method's practical performance, showcasing its ability to handle challenging scenarios with minimal mesh constraints and good agreement with theoretical predictions. These examples highlight the method's versatility in different interface approximations and configurations.

Future work will focus on extending the proposed approach to contact problems involving friction, nonlinear materials, or dynamic interactions. Additionally, exploring further applications of the hybrid interface variable to other types of coupled multiphysics problems, such as fluid–structure interaction or thermal contact, could provide valuable insights and broaden the scope of this method.

In summary, this paper's augmented Lagrangian hybrid Nitsche method offers a flexible, stable, and computationally efficient approach to friction-free contact problems. We believe this framework represents a significant step forward in addressing the challenges associated with contact mechanics and provides a solid foundation for further research and application.

### CRediT authorship contribution statement

Erik Burman: Writing - original draft. Peter Hansbo: Writing - original draft. Mats G. Larson: Writing - original draft.

### Declaration of competing interest

The authors declare that they have no known competing financial interests or personal relationships that could have appeared to influence the work reported in this paper.

### Acknowledgments

This research was supported in part by the Swedish Research Council Grants Nos. 2021-04925, 2022-03908, and the Swedish Research Programme Essence. EB acknowledges funding from EP/T033126/1 and EP/V050400/1.

### Appendix. Additional verifications

In this appendix, we include technical details for the reader's convenience.

• (21). For  $a, b \in \mathbb{R}$ ,

$$a \le 0, \quad b \le 0, \quad ab = 0 \iff a = [a - b]$$
 (103)

**Proof.** 1. Assume that  $a = [a - b]_-$  then we directly have  $a \le 0$ . If a = 0 then  $0 = [0 - b]_- = [b]_+$ , which means that  $b \le 0$  and clearly ab = 0. If a < 0 then a - b < 0 and therefore  $a = [a - b]_- = a - b$  which imply b = 0 and therefore ab = 0.

2. Assume  $a \le 0$ ,  $b \le 0$ , and ab = 0. Then ab = 0 imply either a or b is 0. If a = 0 and  $b \le 0$ , then  $[a - b]_- = [-b]_+ = [b]_+ = 0$ , and it follow that  $a = [a - b]_-$ . If b = 0 and  $a \le 0$  then  $a = [a - b]_- = [a]_-a$ .

• (47). For an affine mapping  $B: \mathbb{R}^n \to \mathbb{R}^m$  it holds

$$||[B(v)]_{-} - [B(w)]_{-}||_{\mathbb{R}^{m}}^{2} \le ([B(v)]_{-} - [B(w)]_{-}, DB(v - w))_{\mathbb{R}^{m}}$$
(104)

**Proof.** Note that, for  $a, b \in \mathbb{R}$ ,

$$([a]_{-} - [b]_{-})(a - b) = [a]_{-}a - [a]_{-}b - [b]_{-}a + b[b]_{-}$$
 (105)

$$\geq [a]_{-}^{2} - 2[a]_{-}[b]_{-} + [b]_{-}^{2} \tag{106}$$

$$=([a]_{-}-[b]_{-})^{2} \tag{107}$$

where we used the identity  $[a]_a = [a]_a^2$ , and the inequality  $[a]_b \le [a]_b^2$ , for  $a, b \in \mathbb{R}$ .

Next for an affine mapping we have

$$DB(v - w) = B(v) - B(w)$$

$$\tag{108}$$

and thus

$$([B(v)]_{-} - [B(w)]_{-}, DB(v - w))_{\mathbb{R}^m}$$
 (109)

$$=([B(v)]_{-}-[B(w)]_{-},B(v)-B(w))_{\mathbb{R}^{m}}$$
(110)

Proceeding component-wise as above, we will directly obtain the estimate.  $\Box$ 

### Data availability

No data was used for the research described in the article.

#### References

- [1] N. El-Abbasi, K.-J. Bathe, Stability and patch test performance of contact discretizations and a new solution algorithm, Comput. Struct. 79 (16) (2001) 1473-1486
- [2] M.A. Puso, T.A. Laursen, A mortar segment-to-segment contact method for large deformations, Comput. Methods Appl. Mech. Engrg. 193 (6–8) (2004) 601–629.
- [3] F. Ben Belgacem, P. Hild, P. Laborde, Extension of the mortar finite element method to a variational inequality modeling unilateral contact, Math. Models Methods Appl. Sci. 9 (2) (1999) 287–303.
- [4] H. Egger, A class of hybrid mortar finite element methods for interface problems with non-matching meshes, 2009.
- [5] E. Burman, D. Elfverson, P. Hansbo, M.G. Larson, K. Larsson, Hybridized cutFEM for elliptic interface problems, SIAM J. Sci. Comput. 41 (5) (2019) A3354–A3380.
- [6] T. Gustafsson, A. Hannukainen, V. Kohonen, J. Videman, Hybrid nitsche for distributed computing, 2025, arXiv:2504.05036.
- [7] R.T. Rockafellar, A dual approach to solving nonlinear programming problems by unconstrained optimization, Math. Program. 5 (1973) 354-373.
- [8] R.T. Rockafellar, The multiplier method of Hestenes and Powell applied to convex programming, J. Optim. Theory Appl. 12 (1973) 555-562.
- [9] R.T. Rockafellar, Augmented Lagrange multiplier functions and duality in nonconvex programming, SIAM J. Control 12 (1974) 268-285.
- [10] F. Chouly, P. Hild, A Nitsche-based method for unilateral contact problems: numerical analysis, SIAM J. Numer. Anal. 51 (2) (2013) 1295–1307.
- [11] E. Burman, P. Hansbo, M.G. Larson, The augmented Lagrangian method as a framework for stabilised methods in computational mechanics, Arch. Comput. Methods Eng. 30 (4) (2023) 2579–2604.
- [12] P. Alart, A. Curnier, A mixed formulation for frictional contact problems prone to Newton like solution methods, Comput. Methods Appl. Mech. Engrg. 92 (3) (1991) 353–375.
- [13] B. Wohlmuth, Variationally consistent discretization schemes and numerical algorithms for contact problems, Acta Numer. 20 (2011) 569-734.
- [14] F. Chouly, M. Fabre, P. Hild, R. Mlika, J. Pousin, Y. Renard, An overview of recent results on nitsche's method for contact problems, in: Geometrically Unfitted Finite Element Methods and Applications, in: volume 121 of Lect. Notes Comput. Sci. Eng., Springer, Cham, 2017, pp. 93–141.
- [15] R. Mlika, Y. Renard, F. Chouly, An unbiased Nitsche's formulation of large deformation frictional contact and self-contact, Comput. Methods Appl. Mech. Engrg. 325 (2017) 265–288.
- [16] F. Chouly, R. Mlika, Y. Renard, An unbiased Nitsche's approximation of the frictional contact between two elastic structures, Numer. Math. 139 (3) (2018) 593–631.
- [17] T. Gustafsson, R. Stenberg, J. Videman, On Nitsche's method for elastic contact problems, SIAM J. Sci. Comput. 42 (2) (2020) B425-B446.
- [18] P. Alart, M. Barboteu, P. Le Tallec, M. Vidrascu, Additive Schwarz method for nonsymmetric problems: application to frictional multicontact problems, in: Domain Decomposition Methods in Science and Engineering (Lyon, 2000), in: Theory Eng. Appl. Comput. Methods, Internat. Center Numer. Methods Eng. (CIMNE), Barcelona, 2002, pp. 3–13.
- [19] Z. Dostál, A. Friedlander, S.A. Santos, Solution of coercive and semicoercive contact problems by FETI domain decomposition, in: Domain Decomposition Methods, 10 (Boulder, CO, 1997), in: volume 218 of Contemp. Math., Amer. Math. Soc., Providence, RI, 1998, pp. 82–93.
- [20] F.J. Cavalieri, A. Cardona, An augmented Lagrangian technique combined with a mortar algorithm for modelling mechanical contact problems, Internat. J. Numer. Methods Engrg. 93 (4) (2013) 420–442.
- [21] S. Hüeber, B.I. Wohlmuth, A primal-dual active set strategy for non-linear multibody contact problems, Comput. Methods Appl. Mech. Engrg. 194 (27-29) (2005) 3147-3166.
- [22] S. Hüeber, B.I. Wohlmuth, An optimal a priori error estimate for nonlinear multibody contact problems, SIAM J. Numer. Anal. 43 (1) (2005) 156-173.
- [23] T.A. Laursen, M.A. Puso, J. Sanders, Mortar contact formulations for deformable-deformable contact: past contributions and new extensions for enriched and embedded interface formulations, Comput. Methods Appl. Mech. Eng. 205/208 (2012) 3–15.
- [24] A. Popp, W.A. Wall, Dual mortar methods for computational contact mechanics—overview and recent developments, GAMM-Mitt. 37 (1) (2014) 66-84.
- [25] M. Tur, J. Albelda, J.M. Navarro-Jimenez, J.J. Rodenas, A modified perturbed Lagrangian formulation for contact problems, Comput. Mech. 55 (4) (2015) 737-754.
- [26] L. De Lorenzis, P. Wriggers, G. Zavarise, A mortar formulation for 3D large deformation contact using NURBS-based isogeometric analysis and the augmented Lagrangian method. Comput. Mech. 49 (1) (2012) 1–20.
- [27] P. Farah, W.A. Wall, A. Popp, An implicit finite wear contact formulation based on dual mortar methods, Internat. J. Numer. Methods Engrg. 111 (4) (2017) 325–353.
- [28] P. Otto, L. De Lorenzis, J.F. Unger, Coupling a NURBS contact interface with a higher order finite element discretization for contact problems using the mortar method. Comput. Mech. 63 (6) (2019) 1203–1222.
- [29] P. Ladeveze, A. Nouy, O. Loiseau, A multiscale computational approach for contact problems, Comput. Methods Appl. Mech. Engrg. 191 (43) (2002) 4869–4891.
- [30] P. Kerfriden, O. Allix, P. Gosselet, A three-scale domain decomposition method for the 3d analysis of debonding in laminates, Comput. Mech. 44 (3) (2009) 343-362.
- [31] D. Zeka, P.-A. Guidault, D. Néron, M. Guiton, On the benefits of a multiscale domain decomposition method to model-order reduction for frictional contact problems, Comput. Methods Appl. Mech. Engrg. 429 (2024) 30, Paper No. 117171.
- [32] E. Burman, P. Hansbo, Deriving robust unfitted finite element methods from augmented Lagrangian formulations, in: Geometrically Unfitted Finite Element Methods and Applications, in: volume 121 of Lect. Notes Comput. Sci. Eng., Springer, Cham, 2017, pp. 1–24.
- [33] S. Claus, P. Kerfriden, A stable and optimally convergent laTIn-cutFEM algorithm for multiple unilateral contact problems, Internat. J. Numer. Methods Engrg. 113 (6) (2018) 938–966.
- [34] P. Hansbo, M.G. Larson, Nitsche's finite element method for model coupling in elasticity, Comput. Methods Appl. Mech. Engrg. 392 (2022) 14, Paper No.
- [35] M. Fabre, J. Pousin, Y. Renard, A fictitious domain method for frictionless contact problems in elasticity using nitsche's method, SMAI J. Comput. Math. 2 (2016) 19–50.
- [36] E. Burman, P. Hansbo, M.G. Larson, R. Stenberg, Galerkin least squares finite element method for the obstacle problem, Comput. Methods Appl. Mech. Engrg. 313 (2017) 362–374.
- [37] V.L. Popov, Contact Mechanics and Friction, Springer-Verlag, Berlin, 2010.
- [38] F.K. Bogner, R.L. Fox, L.A. Schmit, The generation of interelement compatible stiffness and mass matrices by the use of interpolation formulas, in: Proceedings of the Conference on Matrix Methods in Structural Mechanics, Wright Patterson AF Base Ohio, 1965, pp. 397–444.
- [39] P. Hansbo, M.G. Larson, Finite element modeling of a linear membrane shell problem using tangential differential calculus, Comput. Methods Appl. Mech. Engrg. 270 (2014) 1–14.